# Free-Surface Rotational Flow around a Ducted Propeller

Roland Maria-Sube*
*Laboratoire d'Informatique pour la Mecanique et les Sciences de l'Ingenieur, Orsay, France*

**A description of a pseudo-hodographic method for the solution of axisymmetric problems with free boundaries has already been given in a recent publication.[8] This method is now applied to the computation of rotational flows through ducted propellers using the actuator disk approximation. This example involves axisymmetric nonmeridian rotational flows occuring in arbitrary shaped domains. The whole computation involves solutions of several elliptic equations which are carried out using a Galerkin method. The addition of a properly designed duct around a propeller theoretically permits high specific thrusts with compact engines. It can be demonstrated that the improvement of specific thrust is directly related to the downstream fluid diffusion obtained by addition of a duct. The determination of the shape of the downstream free surface generated by the duct is therefore important for the evaluation of the ducted propeller performances. Comparative results are given for irrotational and rotational flows.**

## Nomenclature

$T^*$ = global thrust of the duct-propeller system
$W^*$ = mechanical power of the shaft
$\rho^*$ = density of the incompressible fluid
$\sigma_g$ = $S_4^*/S_2$ = the geometric diffusion
$S_2^*$ = cross-section of the flow at the propeller
$S_4^*$ = cross-section of the jet downstream (Fig. 1)

## Introduction

THE addition of a duct around a propeller has several effects: diminution of the noise; extension of the security for engines moving near ground level; and control of compressibility or cavitation effects on the propeller blades. One of the most significant effects is the increase in the specific thrust of the propeller at low or zero translation speed. One can show,[1,2] using the fundamental theorems of mechanics, that the expression of the thrust $T^*/W^*$, when the propeller is working at zero translation speed and the dissipative effects are not taken into account is

$$\frac{T^*}{W^*} = (2\rho^*)^{1/2} - \left(\frac{2}{T^*/S_4^*}\right)^{1/2} \tag{1}$$

Equation (1) shows that the theoretical value of the specific Thrust $T^*/W^*$, (which does not take into account the dissipative effects), is entirely governed by the ratio $T^*/S_4^*$ in which the cross section of the rotor does not appear. This property emphasizes the interest of a downstream fluid diffusion which, in principle, permits high specific thrusts with compact engines. This characteristic cannot be obtained with classical free propellers.

As a matter of fact, for a free propeller working at zero translation speed, the value of $\sigma_g$ is approximately 0.5; as experimental values of 2.0 and more have been obtained for $\sigma_g$[1] when appropriate ducts are used, we see that significant gains in the specific thrust can thus be obtained.

It must be pointed out however, that in reality, the viscous diffusion causes severe limitations in the gains theoretically available. The geometric diffusion $\sigma_g$ reduces the final ejection speed, (this is favorable for the specific thrust), but increases the average flow speed $\overline{V_7^*}$ in the duct; in consequence, the dissipative losses increase together with the beneficial effects. Experiments, as well as computations including viscosity is extremely sensitive to the viscous losses; a particular care must therefore be taken to minimize these losses in order to protect the gains obtained by diffusion. Nevertheless, a study of the problem within the framework of perfect fluid theory yields useful information concerning the fluid diffusion, the pressure distribution along the duct, and the effects of tangential speed on fluid diffusion. In the following sections, therefore, we shall propose a method for the prediction of the inviscid flow (which can eventually be rotational) around a ducted propeller and of the downstream free surface generated by the duct. In the given examples, the shape of the duct is given, but the method can also handle the inverse problem in which a part of the duct shape may be computed from a given speed distribution.

The theoretical model is defined as follows: the propeller is replaced by an actuator disk of the same diameter. This representation is based on the assumption of the propeller having an infinite number of blades, each blade being represented by a Prandtl lifting line scheme. The original problem, which has an helicoidal symmetry, is thus reduced to an axisymmetric problem. There now exist more sophisticated models than that of the actuator disk, however, we think that this simple model is quite sufficient for ducted propellers in which the number of blades can be large, and in which the volume occupied by the blades does not have a significant influence on the flow. We suppose the fluid to be inviscid and incompressible. The boundaries of the flow are represented in Fig. 2 by their traces on the half meridian plane *xor*; these boundaries will be described in detail in the next section. If the load on the propeller is not constant as the radius varies, then the flow is rotational downstream from the propeller. Furthermore, if the load is large enough, it is necessary to take into account the tangential component of the speed downstream from the propeller. In the next section the governing equations and boundary conditions of the problem will be given.

## II. Formulation of the Problem

As the flow considered is axially-symmetric, the boundaries of the physical domain can be determined by their traces in the meridian plane (Fig. 2). The coordinate system (Fig. 3) includes the axis of symmetry of the flow $\vec{O}x$ and a perpendicular axis $\vec{O}r$ chosen to be tangent to the leading edge of the duct. The meridian traces of the limits are: $\overset{\frown}{AB}$ upstream; $DC$ downstream; and $BC$ and $AGFED$ on both sides of the

Received Dec. 9, 1974; revision received Oct. 24, 1975. This work was achieved at the L.I.M.S.I. (C.N.R.S.) and was partly supported by the "Direction des Recherches et des Moyens d'Essais (D.R.M.E.)" by the Aerospatiale (S.N.I.A.S.) and Bertin Companies. The author wishes to thank Professor M. Holt for his encouragement in the publishing of this paper.

Index categories: Jets, Wakes and Viscid-Inviscid Flow Interactions; Aircraft Subsystem Design.

*Research Scientist.

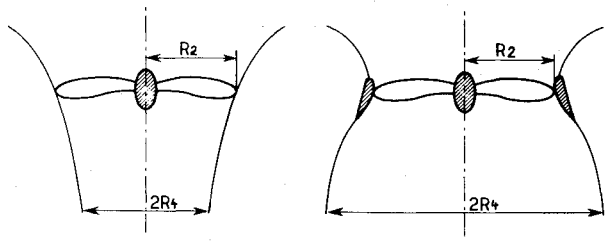


**Fig. 1 Free propeller and ducted propeller slip streams.**

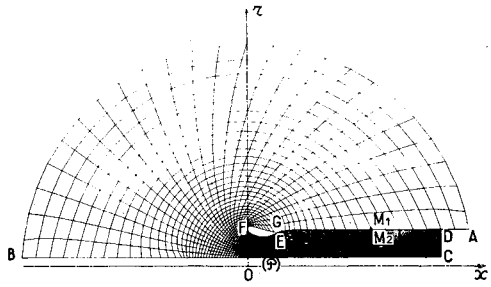


**Fig. 2 Representation of the physical domain by a curvilinear mesh.**

flow. *BC* is the trace of a circular cylinder that gives a schematic representation of the hub of the propeller. The boundary *AGFED* is composed of the meridian trace *EFG* of the duct, and of *AG* and *ED*, which outline the inner and outer faces of the free surface downstream from the duct.

When the computation begins, the shape of the free surface is unknown; a first approximation is chosen arbitrarily (for instance, a simple cylinder). The upstream boundary consists of a spherical section represented by the circular arc $\overset{\frown}{AB}$ in the half meridian plane. The downstream boundary is represented by *CD*. ($\mathcal{P}$) indicates the actuator disk which is perpendicular to $\vec{Ox}$ and those abscissa is $x$. The physical domain ($\mathfrak{D}$) thus delimited, can be divided into two sub-domains: ($\mathfrak{D}_u$) located upstream from the actuator; and ($\mathfrak{D}_d$) downstream from the actuator. It is convenient to use the following subscript to specify some local characteistics of the flow: *0* will refer to the upstream sphere of infinite radius; *1* will refer to the neck plane of the duct; *2* will refer to the actuator circle; *3* will refer to the circle passing through the trailing edge of the duct; and *4* will refer to the plane at infinity downstream.

As the flow considered here is rotational and axisymmetric but nonmeridian, the equation for motion for inviscid incompressible fluids [3-5] may be written

$$\frac{\partial}{\partial x^*}\left(\frac{1}{r^*}\frac{\partial \psi^*}{\partial x^*}\right)+\frac{\partial}{\partial r^*}\left(\frac{1}{r^*}\frac{\partial \psi^*}{\partial r^*}\right)=r^*\left(\frac{dE_a^*}{d\psi^*}-\frac{\gamma^*}{r^{*2}}\frac{d\gamma^*}{d\psi^*}\right) \quad (2)$$

The expression for the meridian speed at point $M$, is thus

$$V^*=\left(\frac{1}{r^*}\frac{d\psi^*}{dn^*}\right) \quad (3)$$

where $n^*$ is the unit vector normal to the stream surface at point $M$. The asterisk shows that the variables concerned are dimensional.

$E_a^*$ is the total energy of a fluid particle of unit mass

$$E_a^*=\tfrac{1}{2}(u^2+v^2+w^2)+\int_0^{\rho^*}\frac{dp^*}{\rho^*} \quad (4)$$

$\gamma^*$ is a function of $\psi^*$ uniquely, called "tangential speed function"[3]

$$\gamma^*(\psi^*)=v^*r^* \quad (5)$$

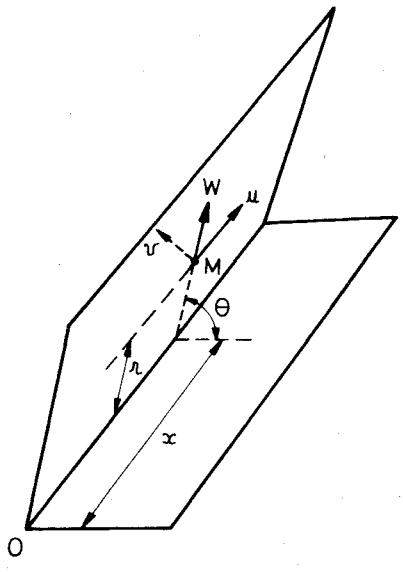


**Fig. 3 Coordinate system.**

Each component of the speed is then given by (Fig. 3)

$$u^*=\frac{1}{r^*}\frac{\partial \psi^*}{\partial r^*},\quad v^*=\frac{\gamma^*}{r^*},\quad w^*=-\frac{1}{r^*}\frac{\partial \psi^*}{\partial^*} \quad (6)$$

In order to deal with dimensionless quantities, let us set

$$x^*=xR_1^*,\quad \psi^*=\overline{V}_1R_1^{*2}\psi,\quad \gamma^*=\overline{V}_1^*R_1^*\gamma,$$

$$r^*=rR_1^*,\quad E_a^*=\overline{V}_1^{*2}E_a$$

where $R_1^*$ is the radius of the neck of the duct and $\overline{V}_1^*$ is the mean meridian speed through that section. The right hand side of (2) vanishes in ($\mathfrak{D}_u$) where the flow is purely meridian and irrotational. In ($\mathfrak{D}_d$), the derivatives $dE_a/d\psi$ and $d\gamma/d\psi$ are identical to $d(\delta E_a)/d\psi$ and $d(\delta\gamma)/d\psi$ respectively, where the symbol $\delta$ denotes the jump through the actuator of the accompanying function.

From Euler's theorem, we have

$$\delta E_a=\Omega\delta\gamma=\Omega vr \quad (8)$$

where $\Omega$ is the reduced angular speed of the disk

$$\Omega^*=\Omega\overline{V}_1^*/R_1^*$$

$\Omega^*$ is the angular speed of the disk. Another parameter in current use is $\lambda$, the inverse of $\Omega$.

Finally, the equation governing the flow is

$$\frac{\partial}{\partial x}\left(\frac{1}{r}\frac{\partial \psi}{\partial x}\right)+\frac{\partial}{\partial r}\left(\frac{1}{r}\frac{\partial \psi}{\partial r}\right)=\left(r-\frac{\delta E_a}{\Omega^2 r}\right)\frac{d}{d\psi}\left(\delta E_a\right) \quad (9)$$

Let us set

$$S(\psi)=\left(r-\frac{\delta E_a}{\Omega^2 r}\right)\frac{d}{d\psi}\left(\delta E_a\right)$$

When the flow is meridian, the term $\delta E_a/\Omega^2 r$ vanishes. The components of the speed are given by

$$u(\psi)=\frac{1}{r}\frac{\partial \psi}{\partial r} \quad (10a)$$

$$v(\psi)=\frac{1}{r\Omega}\delta E_a(\psi) \quad (10b)$$

$$w(\psi) = -\frac{1}{r}\frac{\partial \psi}{\partial x} \tag{10c}$$

The boundary conditions are

$$\psi = 0 \quad \text{on } BC \tag{11a}$$

$$\psi = \tfrac{1}{2} \quad \text{on } DEFGA \tag{11b}$$

$$\frac{d\psi}{dn} = 0 \quad \text{on } CD \text{ and } \widehat{BA} \tag{11c}$$

The condition on $\widehat{BA}$ is only an approximation since the correct condition would be $d\psi/dn = 0$ one the sphere of infinite radius. The balance condition on the free boundary, expressed in terms of static pressure is

$$p_{M_1} - p_{M_2} = 0 \tag{12}$$

for every $M_1 \epsilon GA$ and $M_2 \epsilon ED$ where $M_1$ and $M_2$ are a pair of points located on the free surface, one on the external side the other on the internal side, which are infinitely close together.

Using Bernoulli's relation for incompressible flows, Eq. (12) may be written

$$\tfrac{1}{2}(u^2+w^2)_{M_1} - \tfrac{1}{2}(u^2+v^2+w^2)_{M_2} + \frac{v_{M_2}^2}{r_{M_2}} + \delta E_a = 0 \tag{13}$$

for every $M_1 \epsilon AG$ and $M_2 \epsilon ED$.

The Kutta-Joukowski condition sets the slip-stream to intiate at the trailing edge $E$. This leads us to let $\delta E_a$ vary freely in Eq. (13); therefore we shall replace this quantity by an unknown constant $k$. Moreover, it can be noticed that for the problem considered here, the quantity $(u^2+v^2)_{M_1}$ vanishes on $G$ and remains close to zero on $GA$. Finally, the expression of the balance condition is:

$$\tfrac{1}{2}(u^2+v^2+w^2)_{M_2} - \left(\frac{v^2}{r}\right)_{M_2} = k \quad \text{for } M_2 \epsilon ED \tag{14}$$

Equation (14) shows that for meridian flows ($v_{M_2} = 0$), the slip stream must be tangent to the inner surface of the duct at point $E$.

## III. Numerical Solution of the Problem

The problem formulated in the last section now calls for two remarks: first, the governing equation (9) is nonlinear since the right hand side depends on the solution; and second the problem involves unknown boundaries.

A numerical solution of this problem is proposed using a double loop successive approximations procedure on the right hand side of Eq. (9) and on the free boundary geometry.[7,8] At each step of this procedure, one has to solve a Poisson problem defined inside a given domain. This computation is carried out using an isoparametric Galerkin method described in Refs. (6-8).

As a consequence of the fact that $\delta E_a$ is unknown, a successive approximation procedure (see Sec. IV) must be used for the computation of $S(\psi)$. The computational scheme of the complete problem is shown in Fig. 4. First, a solution of the meridian flow problem, for which only the derivative of $\delta E_a$ needs to be known, is computed (solid line path); the corresponding procedure implies two loops of successive approximations, the inner loop iterates on the right hand side of Eq. (9) while the outer loop iterates on the free boundary shape. The solution thus obtained for the meridian flow problem gives a first approximation of the function $\delta E_a(\psi)$ which is used to initialize the computation of the problem governed by Eq. (9). This solution is computed using the algorithm indicated by the dotted line path (Fig. 4).

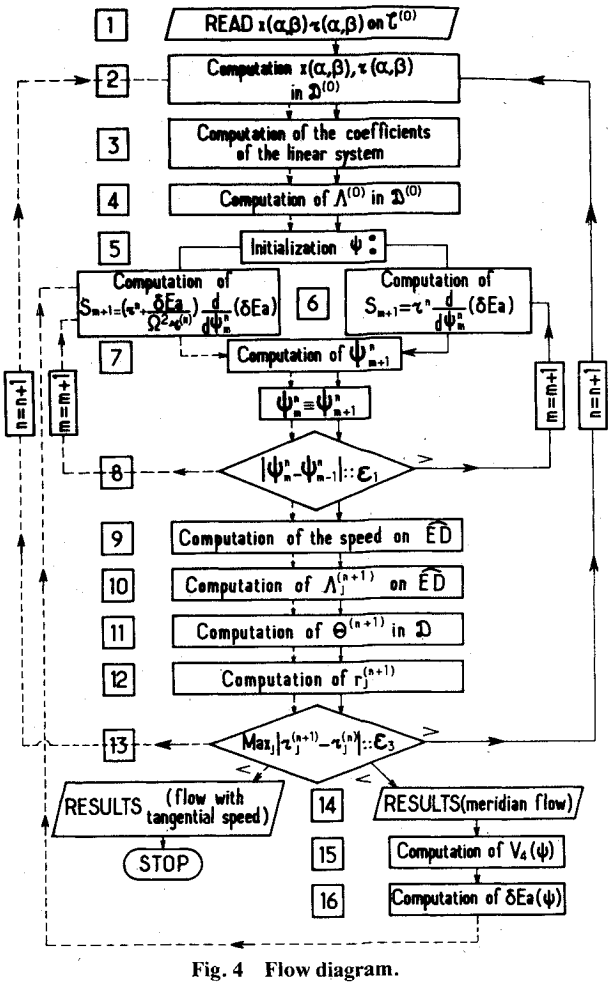


Fig. 4 Flow diagram.

The enumeration of the steps of the computation is as follows: 1) the value of $x$ and $r$ are read at each node of (C). An arbitrary initial shape has been given to the free surface; 2 and 3) Computation of a curvilinear mesh (Fig. 2) and of the coefficients of the linear system approximating the Poisson problem is performed. 4) the analytical function Log $\mathfrak{M}$ (defined in Sec. V) is computed in ($\mathfrak{D}$); 5) $\psi$ is initialized in ($\mathfrak{D}$); 6-8) the second member $S(\psi)$ is computed by the successive approximations procedure described in Sec. IV; 9-12) a new approximated shape of the jet boundary is determined (Sec. 4); and 13) the meridian flow problem has been solved.[14-16] From the values of $V_4$ then computed downstream, one can determine the function $\delta E_a(\psi)$. Returning to step 6) and following the dotted line path, another procedure of successive approximations of $\delta E_a(\psi)$ is necessary to carry out the computation of the nonmeridian flow.

## IV. Computation of $S(\psi)$

In the general case of a flow having a tangential component, the expression for $S$ is

$$S(\psi) = \left(r - \frac{\delta E_a}{\Omega^2 r}\right)\frac{d}{d\psi}(\delta E_a)$$

As pointed out in Section III, $\delta E_a(\psi)$ cannot be given arbitrarily since this data would generally not be compatible with the assumption that the separation point of the inner flow takes place at the trailing edge $E$. Moreover, $d/d\psi(\delta E_a)$ is generally not known either, since in most practical problems the only given function is $d/dr(\delta E_a)|_{x=x0}$ on the actuator disk. Therefore, $S(\psi)$ has to be computed by a procedure of successive approximations, as follows: to start the computation, we first make the assumption that the flow is

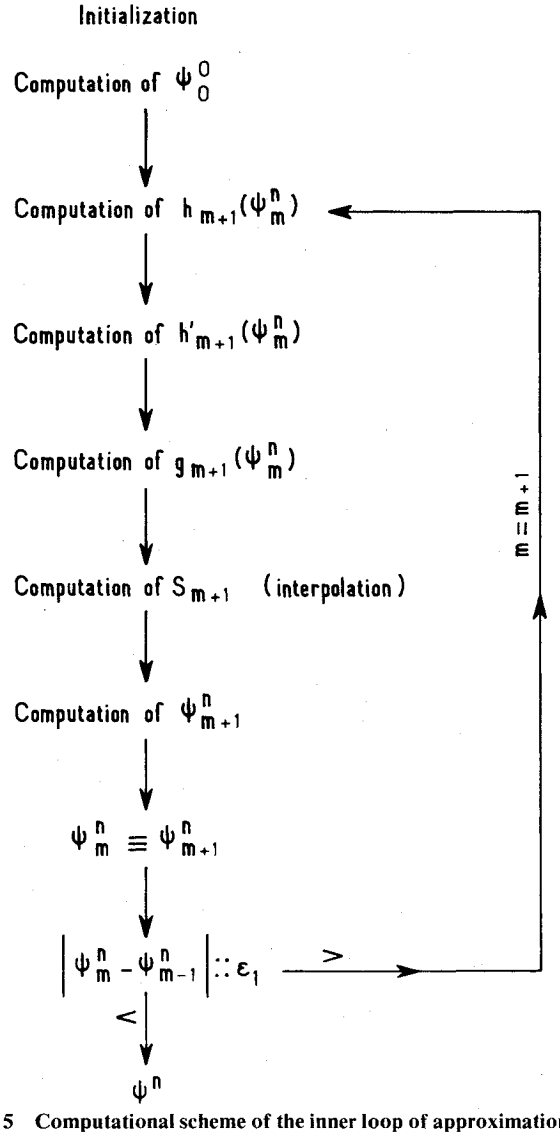


**Fig. 5 Computational scheme of the inner loop of approximations.**

meridian; the tangential term vanishes and the expression for $S(\psi)$ reduces to

$$S(\psi) = r\frac{d}{d\psi}(\delta E_a) \tag{16}$$

where $\delta E_a = \delta p/\rho$ is a function of $\psi$. We suppose that, on the actuator disk, we have

$$\frac{d}{dr}(\delta E_a)\Big|_{x=x_0} = f(r) \tag{17}$$

$f$ is given and $x_0$ is the abscissa of the disk. Let us set

$$\frac{d}{d\psi}(\delta E_a) = g(\psi) \tag{18}$$

$g \equiv 0$ in $(\mathfrak{D}_u)$ and is unknown in $(\mathfrak{D}_d)$. Let us suppose that $\psi(x,r)$ is known in $(\mathfrak{D}_d)$, then, for $x = x_0$, $r = h(\psi)$ is known. Since

$$\frac{d}{d\psi}(\delta E_a)\Big|_{x=x_0} = \frac{\partial/\partial r(\delta E_a)}{\partial\psi/\partial r}\Big|_{x=x_0} \tag{19}$$

One can find $g(\psi)$, knowing that $\delta E_a$ only depends on $\psi$

$$g(\psi) = f[h(\psi)] \cdot h'(\psi) \tag{20}$$

The algorithm of the computation is illustrated by Fig. 5. The procedure consists of successive approximations starting from given initial values $\psi_0^0$ for the stream function. In practice $\psi_0^0(x,r)$ is chosen to be the stream function of the corresponding irrotational flow. Knowing $\psi_0^0(x_0,r)$, the determination of $h_1(\psi_0^0)$ and $h_1'(\psi_0^0)$ can be obtained; $g_1(\psi_0^0)$ is then determined using Eq. (20); $S_1$ can then be obtained, and $\psi_1^0$ is computed by solving Eq. (21)

$$\frac{\partial}{\partial x}\left(\frac{1}{r}\frac{\partial\psi_1^0}{\partial x}\right) + \frac{\partial}{\partial r}\left(\frac{1}{r}\frac{\partial\psi_1^0}{\partial r}\right) = S_1 \tag{21}$$

Another loop is then carried out, and so on until the test

$$\operatorname{Max}_{(\mathfrak{D}_d)} |\varphi_m^0 - \varphi_{m-1}^0| < \epsilon_1$$

is satisfied.

$$\frac{\partial}{\partial x}\left(\frac{1}{r}\frac{\partial\psi_1^0}{\partial x}\right) + \frac{\partial}{\partial r}\left(\frac{1}{r}\frac{\partial\psi_1^0}{\partial r}\right) = S_1 \tag{21}$$

Another loop is then carried out, and so on until the test

$$\operatorname{Max}_{(\mathfrak{D}_d)} |\varphi_m^0 - \varphi_{m-1}^0| < \epsilon_1$$

is satisfied.

Once the free surface has been determined, (Eqs. 9 to 14) for a meridian flow, the function $\delta E_a(\psi)$ can be determined for the computed meridian flow; for every stream surface the Bernoulli equation gives

$$\tfrac{1}{2}(u_4^2 + w_4^2) + \frac{p_4}{\rho} = \tfrac{1}{2}(u_0^2 + w_0^2) + \frac{p_0}{\rho} + \frac{\partial p}{\rho} \tag{22}$$

where the subscripts *0* and *4* refer to upstream and downstream conditions respectively. $\delta p$ is the discontinuity of pressure through the actuator. The balance condition sets $p_4$ to be equal to $p_0$ on the free surface; $p_4$ is thus equal to $p_0$ for every value of $\psi$; since $u_0$ and $w_0$ are infinitely small, and since $w_4$ vanishes, Eq. (22) gives

$$\delta E_a(\psi) = \tfrac{1}{2}[u_4(\psi)]^2 \tag{23}$$

The function $\delta E_a(\psi)$ thus determined can be taken as a first approximation in evaluating (step 6) the function $\gamma(\psi)$ and the right hand side of the nonmeridian flow equation of motion

$$S(\psi) = \left(r + \frac{\delta E_a}{\Omega^2 r}\right)\frac{d}{d\psi}(\delta E_a) \tag{24}$$

After another procedure of successive approximations on the free surface (steps 6-14), new values can be computed for $\delta E_a(\psi)$, as follows

$$\tfrac{1}{2}(u_4^2 + v_4^2) + \frac{p_4}{\rho} = \tfrac{1}{2}(u_0^2 + w^2{}_0) + \frac{p_0}{\rho} + \frac{\delta p}{\rho} \tag{25}$$

where $u_0$ and $w_0$ can be neglected. $\Delta E_a(\psi)$ is then given by expression (26)

$$\delta E_a(\psi) = \tfrac{1}{2}\{[u_4(\psi)]^2 + [v_4(\psi)]^2\} + \frac{p_4(\psi) - p_0(\psi)}{\rho} \tag{26}$$

with

$$\frac{p_4(\psi) - p_0(\psi)}{\rho} = -\frac{v^2}{R_4}\Big|_{\psi=\frac{1}{2}} - \int_{R_4}^{r_4}\frac{[v_4(\psi)]^2}{r_4(\psi)}dr \tag{27}$$

**Table 1 Global results obtained for various working cases.**

| | IRROTATIONAL MERIDIAN ($\lambda=0$) | ROTATIONAL MERIDIAN ($\lambda=0$) | ROTATIONAL ($\lambda=0.5$) | ROTATIONAL ($\lambda=1.33$) |
|---|---|---|---|---|
| $\sigma_G$ | 1.51 | 1.56 | 1.56 | 1.58 |
| $\sigma_F$ | 1.25 | 1.325 | 1.325 | 1.34 |
| T | 2.14 | 2.12 | 2.105 | 2.07 |
| W | 0.73 | 0.715 | 0.74 | 0.85 |
| $T/W$ | 2.94 | 2.96 | 2.84 | 2.43 |
| m | 1.23 | 1.23 | 1.18 | 1.00 |

We recall the relation existing between $v_4(\psi)$, $r_4(\psi)$ and $\delta E_a(\psi)$

$$v_4(\psi)=\frac{1}{\Omega}\cdot\frac{rE_a(\omega)}{r_4(\psi)} \tag{28}$$

If $\ell$ denotes the rank of the approximation on $\delta E_a(\psi)$ then Eqs. (26-28) give, for the expression of $\delta E_a^{(\ell+1)}(\psi)$

$$\delta E_a^{(\ell+1)}(\psi)=\tfrac{1}{2}[u_4(\psi)]^2+\left[\frac{\delta E_a^{\ell}(\psi)}{\Omega.r_4(\psi)}\right]\cdot\left(\tfrac{1}{2}-\frac{1}{R_4}\right)$$
$$+\int_{r_4(\psi)}^{R_4}\left[\frac{\delta E_a^{\ell}}{\Omega r_4(\psi)}\right]\frac{dr_4}{r_4(\psi)} \tag{29}$$

where $R_4$ is the radius of the jet cross section, downstream. The procedure of successive approximations is stopped when inequality Eq. (30) is satisfied

$$\max_{(\mathfrak{D}_d)}|\delta E_a^{\ell+1}-\delta E_a^{\ell}|\leq\epsilon_2 \tag{30}$$

where $\epsilon_2$ is a given upper bound.

## V. Computation of the Jet Boundary

The principle of the method used for the determination of the jet boundary has been described in a recent paper.[8] This heuristic method is one among several others using a successive approximations procedure,[9] however, its main characteristic is to possess a great computational stability, whereas point by point methods lead to computational instability and require smoothing techniques. We shall describe now the equations specific to the example examined in this paper, involving axisymmetric rotational flows with a tangential component.

As seen in Sec. II, the balance condition on the jet boundary can be written in the form of Eq. (13) with

$$u=\frac{1}{r}\frac{\partial\psi}{\partial x},\quad v=\frac{\delta E_a}{\Omega r},\quad w=-\frac{1}{r}\frac{\partial\psi}{\partial r}$$

and $k$ constant for $\forall M_2$ on $\widehat{ED}$.

Condition (13) may also take the form

$$V_{M_2}^2-K=0\quad\text{for }\forall M_2\text{ on }\widehat{ED} \tag{31}$$

with

$$V=\frac{1}{r}\frac{d\psi}{dn}=(u^2+w^2)^{1/2}$$

and

$$K=\left(\frac{\delta E_a}{\Omega}\right)_{M_2}^2\cdot\left(\frac{1}{r^3}-\frac{1}{2r^2}\right)_{M_2}+k \tag{32}$$

Let us now consider an analytic function $F=\alpha+i\beta$ which realizes a conformal mapping of $(\mathfrak{D})$ on a rectangle $(\overline{\mathfrak{D}})$, such that $\beta$ remains constant on the boundaries of the flow while $\alpha$ keeps constant on the upstream and the downstream limits. Let $\mathfrak{M}$ and $\theta$ be the modulus and the argument of $dF/dz$, $(z=x+ir)$. The expression of the meridian speed at every point of $\widehat{ED}$, can be written

$$V_{M_2}=\left(\frac{\mathfrak{M}}{r}\frac{d\psi}{d\beta}\right)_{M_2} \tag{33}$$

From Eqs. (31) and (32), one obtains the following condition for $\mathfrak{M}$

$$\mathfrak{M}=\sqrt{K}/\left(\frac{1}{r}\frac{d\psi}{d\beta}\right) \tag{34}$$

This relation associates with the speed distribution along the jet boundary a quantity $\mathfrak{M}$ connected to the shape of this boundary, and leads consecutively to the following iterative procedure for fulfilling the balance condition

$$\mathfrak{M}^{(n+1)}=\frac{\mathfrak{M}^{(n)}}{V^{(n)}}\sqrt{K} \tag{35}$$

where $K$ is determined by Eq. (32) and $(n)$ denotes the number of iterations on the jet shape.

When the distribution Log $\mathfrak{M}^{(n+1)}$ has been determined by Eq. (36), the associated conjugate function $\theta^{(n+1)}$ is computed by solving an elliptic problem in $(\mathfrak{D})$. One then obtains the $(n+1)^{st}$ approximated shape on the jet boundary by integrating Eq. (36)

$$dx^{(n+1)}=[\cos\theta^{(n+1)}]/\mathfrak{M}^{(n+1)}d\alpha$$
$$dy^{(n+1)}=[\sin\theta^{(n+1)}]/\mathfrak{M}^{(n+1)}d\alpha \tag{36}$$

The loop of the approximations is ended when inequality Eq. (37) is satisfied.

$$\text{Max}_{ED}|r^{(n+1)}-r^{(n)}|<\epsilon_3 \tag{37}$$

About ten iterations are required for $E_3\sim 0.001$.

## VI. Results

The computations were carried out using the 2100 nodes mesh shown on Fig. 2. Comparative results are given in Figs. (7 to 10) for the three following cases admitting the same solid boundaries (Figs. 2 and 8) and having the same average stream velocity, i.e.: the irrotational meridian flow; the rotational nonmeridian flow with $\lambda=0.5$ (propeller weakly loaded); and the rotational non-meridian flow with $\lambda=1.33$ (propeller normally loaded). The two rotational flows follow the same given law

$$f(r)=\frac{\partial}{\partial r}(\delta E_a)|_{x=x_0}$$

(Fig. 6) where $\delta E_a$ is the jump of total energy through the actuator disk. The resulting distributions $\delta E_a(\psi)$, computed for each case, are shown in Fig. 7. It should be pointed out here, that more general laws than the one given in Fig. 6 are compatible with the method used for the solution of the problem. Figure 8 gives the computed shapes of the jet boundary for each aforementioned case and the corresponding values of the speed on the inner and outer surfaces of the duct and on the jet boundary. Figures 9 and 10 show the axial, radial and tengential components of the velocity computed in the actuator plane and the plane downstream, respectively. From these results, it is easy to compare (Table 1) the geometric diffusion $\sigma_g$ and the fluid diffusion $\sigma_f$ obtained for each case. We recall here that: $S_2$ is the cross section of the flow at the propeller; $S_3$ is the cross section of the flow at the trailing-

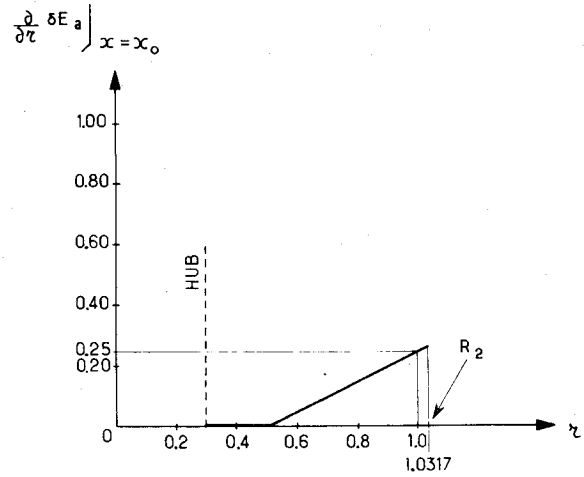


Fig. 6 Given variation of the total energy along the actuator radius.

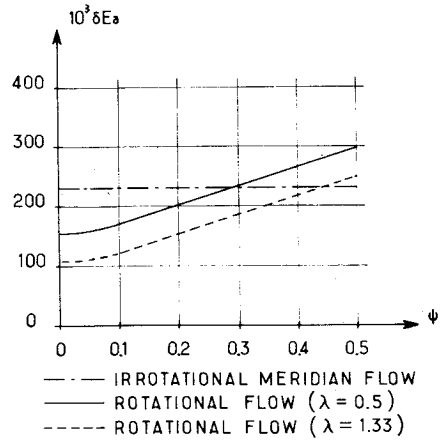


Fig. 7 Computed values of the total energy plotted against the stream function.

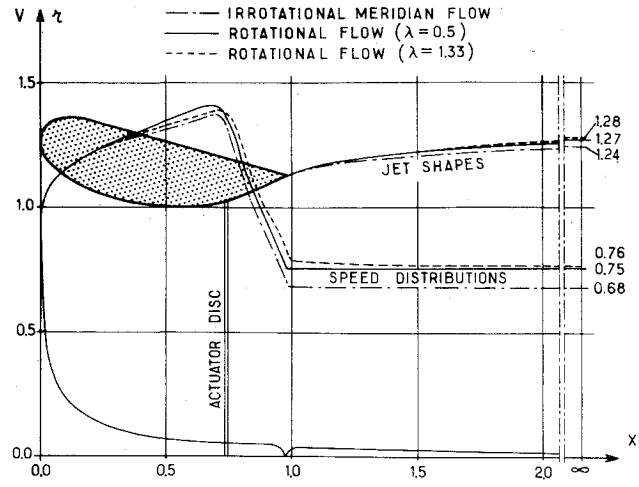


Fig. 8 Speed distribution on the duct and along the jet boundary.

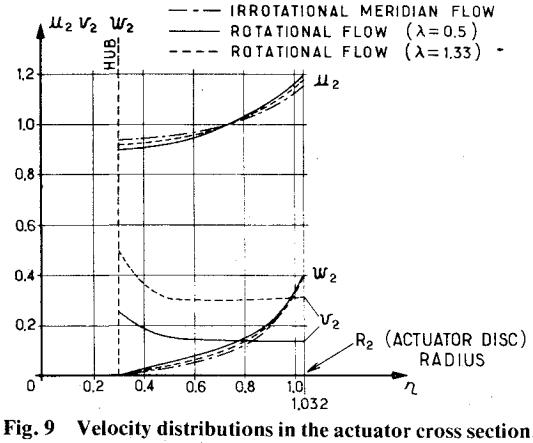


Fig. 9 Velocity distributions in the actuator cross section.

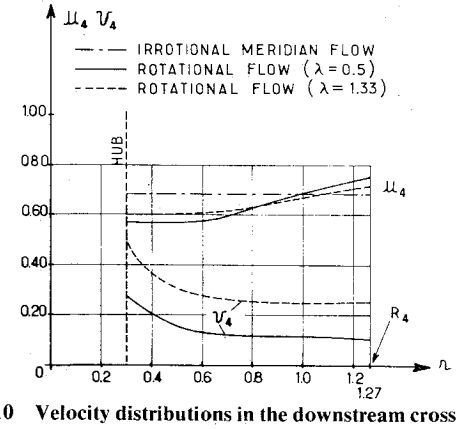


Fig. 10 Velocity distributions in the downstream cross section.

edge of the duct; and $S_4$ is the cross section of the jet at infinity downstream.

The global thrust $T^*$ given by the duct-propeller system and the mechanical power $W^*$ transmitted to the propeller is obtained from Eqs. (38) and (39)

$$T^* = \rho^* \int_{CD} u_4^{*2} dS_4^* = \rho^* \overline{V_1^*}^2 R_1^{*2} T \tag{38}$$

$$W^* = \frac{\rho^*}{2} \int_{CD} (u_4^{*2} + v_4^{*2} + w_4^{*2})^{3/2} dS_4 = \rho^* \overline{V_1^*}^3 R_1^{*2} W \tag{39}$$

where $T$ and $W$ are dimensionless parameters and $\rho^*$, $\overline{V_1^*}$ and $R_1^*$, are the reference quantities defined in Sec. II.

The following dimensionless ratios can be obtained from $T^*$ and $W^*$, i.e.,

$$\frac{T}{W} = \frac{T^*}{W^*} \cdot \overline{V_1^*} \tag{40}$$

and the figure of merit

$$m = \frac{T^{*3/2}}{2(\rho^* S_2^*)^{1/2} W^*} = \frac{T^{3/2}}{2W} \cdot \frac{R_1^*}{(S_2^*)^{1/2}} \tag{41}$$

Table 1 gives the values of $\sigma_g$, $\sigma_f$, $T$, and $W$ for each of the three aforementioned cases plus the rotational meridian flow following the law $f(r)$ of Fig. 6. These results obtained with ideal flows call for the following remarks: the effects of rotationality and of the tangential component of the motion both result in an increase of the diffusion, however, this gain is more than counteracted by the negative effects of the tangential motion, even when the dissipative effects are not taken into account. This illustrates the well known fact that significant gains in efficiency can be obtained by redressing the flow downstream from heavily loaded propellers. Experimental results have shown that in this latter case, the beneficial effects due to the elimination of the tangential motion are more significant than the additive dissipative effects due to the redress.

Lastly, recall that the figure of merit $m$ has the same meaning as an efficiency, it may however take values greater than 1 due to the effect of diffusion in the case considered, while the referring case is irrotational meridian with a diffusion equal to 1.

An interesting property of our computational method lies in its capacity to solve mixed problems with both direct and inverse conditions on the boundary; the procedure used for the determination of the jet boundary could be used in the same manner for the determination of a solid boundary defined by a pressure or a velocity distribution. This possibility is of particular interest when appropriate shapes of the duct have to be found, especially near the trailing edge in order to avoid separation. Though no illustration of this application is given here, such a computation could be done readily by the numerical program we have used for the solution of the aforementioned examples.

These computations were carried out on a UNIVAC 1108 system. About 16 minutes of central unit time are required to solve successively the irrotational problem, the rotational meridian problem, and one case of the non-meridian rotational problem. The program is written in FORTRAN V language and comprises nearly 2000 statements.

## VII. Conclusions

The results presented in this paper have brought useful information to the engineers in charge of the design and development of a VTOL aircraft propulsion system. These results have given important indications in the conducting of experimental investigations.

As an extension of the theoretical model presented in this paper, mention is made of the possibility of coupling this model with a classical boundary layer calculation along the duct.

From a computational point of view, the examples presented in this paper give a new illustration of the versatility of a method we have developed for the computation of free boundary axisymmetric flows of ideal fluids. These examples emphasize the efficiency of the harmonic curvilinear mesh and Galerkin method when physical domains are arbitrarily shaped. With the problems treated in this paper and in Ref. (8), we have presented two examples involving free boundary problems of incompressible rotational flows. Since then, the method has been applied to compressible irrotational flows with free-surface[10] and to flows with free surface and gravity.[11] Presently, the method is being applied to the solution of after-body problems which involve free boundaries with rotational compressible flows.

## References

[1] Lazareff, M., "Etudes Aerodynamiques Generales des Helices Carenees," *SNIAS Report ARA/NT/89/67*, private communication, Feb. 1967.

[2] Kuchemann, D. and Weber, Jr., *Aerodynamics of Propulsion*, McGraw-Hill, N.Y. 1953, pp. 125-139.

[3] Siestrunck, R. and Fabri, J., "Ecoulements Tourbillonnaires dans les Machines Axiales," *ONERA* Publication No. 45, 1950.

[4] Wu Chung Hua, "A General Theory of Fluid Flow with Subsonic or Supersonic Velocity in Turbomachines of Arbitrary Hub and Casing Shapes," *NACA*, T.N. 2302, 1951.

[5] Milne-Thomson, L. M., *Theoretical Hydrodynamics*, 5th edition, MacMillian Press, N. Y., 1968, pp. 106-120.

[6] Bellevaux, C., "Oscillation Propre d'un Bassin Tournant. Courant Induit par le Vent sur un Bassin," *These de Doctorat d'Etat*, A.O. 4407 Universite de Paris, Paris, May 1970.

[7] Bellevaux, C. and Maria Sube, R., "Determination de Lignes de Jets dans des Ecoulements Rotationnels Axisymetriques – 2$^{eme}$ partie: Resolution numerique, *Journ. Mec. 11*, No. 1, mars 1972.

[8] Maria-Sube, R., "Numerical Solution to Free-Surface Axisymmetric Rotational Flows," *Journal of Computer Physics*, Vol. 16, Oct. 1974, pp. 127-149.

[9] Cryer, C. W., "On the Approximate Solution of Free Boundary Problems Using Finite Differences," *Journal of the Association of Computer Machines*, Vol. 17, 1970.

[10] Maria-Sube, R., Chattot, J. J., and Gillon, G., "Couplage Entre l'Ecoulement Autour d'un Arriere-Corps et le Jet Propulsif en Theorie de Fluide Parfait," A.G.A.R.D. Symposium on Airframe/Propulsion Interference, Rome, Sept. 1974.

[11] Maria-Sube, R., "Resolution par une Methode d'Elements Finis, de Problemes de Jets Axisymetriques en Ecoulement de Fluide Pesant," Comptes Rendus Ac. Sc. no 281 serie B, presentee le 23 juin 1975, pp. 333-336.